Eruption Types and Conduit Dynamics of Kukusan and Genteng Volcanoes of the Ijen Volcanic Complex, Indonesia

Mitsuoka, Takeru
Department of Earth and Planetary Sciences, Graduate School of Science, Kyushu University

Toramaru, Atsushi
Department of Earth and Planetary Sciences, Graduate School of Science, Kyushu University

Harijoko, Agung
Department of Geological Engineering, Faculty of Engineering, Universitas Gadjah Mada

Haryo Edi Wibowo
Department of Geological Engineering, Faculty of Engineering, Universitas Gadjah Mada

https://doi.org/10.5109/4371995

出版情報：九州大学大学院理学研究院紀要 : Series D, Earth and planetary sciences. 35 (1), pp.1-17, 2021-03-26. 九州大学大学院理学研究院
バージョン：
権利関係：

Mem. Fac. Sci., Kyushu Univ., Ser. D, Earth & Planet. Sci., Vol. XXXV, No. 1,
pp. 1-17, March 26, 2021

Eruption Types and Conduit Dynamics of Kukusan and Genteng Volcanoes of the Ijen Volcanic Complex, Indonesia

Takeru Mitsuoka[1], Atsushi Toramaru[1], Agung Harijoko[2], and Haryo Edi Wibowo[2]

Abstract

Eruption mechanisms of mafic magma are strongly debated, especially the mafic Plinian eruption. Few examples of mafic Plinian eruptions prevent us from knowing what condition causes rapid magma ascent and degassing processes. Kukusan and Genteng volcanoes, which are monogenetic volcanoes in the Ijen caldera complex in Indonesia, produced explosive eruptions of mafic magma. Their chemical compositions are similar, but the volcanoes are believed to have different eruption types. Therefore, these volcanoes were chosen to reveal the factors affecting the eruption types of mafic magma. Outcrops were observed at 31 locations in fieldwork. Geochemistry, petrography, and microtextural analyses of scoria were conducted. Based on the dispersal area and fragmentation degree of the volcanic deposits, the eruption type of Kukusan is considered as sub-Plinian, while that of Genteng is considered as Strombolian. The microtextural analysis showed that the Kukusan scoria had a higher bubble number density (BND), microlite number density (MND), and microlite crystallinity than the Genteng scoria. High BND and MND values suggest rapid decompression, i.e. rapid magma ascent in the volcanic conduit. High microlite crystallinity indicates high magma viscosity. The higher ascent rate and higher viscosity of the Kukusan magma suggest coupled degassing and fragmentation, leading to a more explosive sub-Plinian eruption. In contrast, the lower ascent rate and lower viscosity of the Genteng magma suggests decoupled degassing, which leads to a Strombolian eruption.

Keywords: ascent rate; degassing process; scoria; bubble number density; microlite crystallinity

I. Introduction

Explosive volcanic eruptions are classified by the dispersal area and fragmentation degree of pyroclastic deposits (Walker 1973). Generally, mafic magma generates Hawaiian or Strombolian eruptions, and rarely Plinian eruptions (Kereszturi and Nemeth 2012). However, it has been recently recognized that mafic magma sometimes produces a Plinian eruption. Some examples of mafic Plinian eruptions include Etna 122 BC in Italy (Sable et al. 2006), Tarawera 1886 in New Zealand (Houghton et al. 2004), and Pleistocene Fontana Lapilli in Nicaragua (Costantini et al. 2010). Determining the mechanisms that cause various types of eruptions is critical for the hazard mitigation of highly explosive eruptions. Three mechanisms are thought to control mafic Plinian eruptions: rapid magma ascent, coupled degassing, and brittle fragmentation (Sable et al. 2006, Houghton and Gonnermann 2008, Costantini et al. 2010). Weakly explosive style of mafic magma is believed to be associated with decoupled degassing, in which bubbles are able to migrate upward within relatively slow ascending melt, whereas highly explosive style of silicic or mafic magma is believed to be associated with coupled degassing, in which bubbles are immobile relative to the melt (Sable et al. 2006). However, few examples of mafic Plinian eruptions prevent us from knowing what condition causes rapid magma ascent and coupled degassing.

Kukusan and Genteng volcanoes form part of the Ijen Caldera Complex in East Java, Indonesia. Kukusan and Genteng produced explosive eruptions of mafic magma at between 21 and 2 ka (Sitorus 1990, Sundhoro 1990,

1 Department of Earth and Planetary Sciences, Graduate School of Science, Kyushu University, Japan
2 Department of Geological Engineering, Faculty of Engineering, Universitas Gadjah Mada, Indonesia

Suhendro et al. 2016). Although some researchers studied the Ijen Caldera Complex, they did not map the dispersal area nor conduct a textural analysis of pyroclastic deposits. Drawing a dispersal map of volcanic deposits will contribute to volcanic hazard assessment. In this study, we aim to determine the eruption types of Kukusan and Genteng volcanoes. Kukusan and Genteng volcanoes are located in the same caldera and have similar chemical compositions. The eruption types of Kukusan and Genteng are unknown but are thought to be different based on geological map (Sujanto et al. 1988). Therefore, the pyroclastic deposits of Kukusan and Genteng are herein used to compare their magma properties, which likely affect the eruption types. The textural analysis of bubbles and crystals provides information on magma ascent, degassing, and fragmentation in a volcanic conduit. The study of the conduit dynamics of Kukusan can add a case example of mafic Plinian eruption, as well as describe the conditions that cause rapid magma ascent, coupled/decoupled degassing, and fragmentation. In this study, we aim to understand the factors that have an effect on their explosive eruption of mafic magma by comparing the cases of Kukusan and Genteng volcanoes.

Section 2 presents the geological settings of the Ijen Caldera Complex. In Section 3, we outline the methods utilized in this study. Section 4 reports the fieldwork results and provides the laboratory analyses of the Kukusan and Genteng pyroclastic deposits. Finally, we interpret the obtained results and discuss the relationship between conduit dynamics and the Kukusan and Genteng eruption types.

II. Geological settings

Java Island is located in the subduction of the Indian-Australian plate beneath the Eurasian plate (Hamilton 1979). The Ijen Volcanic Complex is located in the easternmost part of Java Island (Fig. 1) within the Quaternary volcanic front of the Sunda arc. The volcanic complex features a caldera rim on the northern boundary, five stratovolcanoes on the southern boundary, and several post-caldera monogenetic volcanoes within the intra-caldera plane (Caudron et al. 2015). The Ijen caldera's diameter is 18 km in the east-west direction and 15 km in the north-south direction. The caldera formation occurred between 294 and 50 ka (Sitorus 1990). The post-caldera eruption formed over 22 separate vents. The vents are separated geographically into two groups: the caldera rim group and the intra-caldera group (Handley et al. 2007). Post-caldera volcanic deposits represent various rock types: lava, pyroclastic flow, pyroclastic air fall and surge deposits (Sitorus 1990). Kukusan and Genteng are monogenetic volcanoes located inside the Ijen caldera. Kukusan is approximately 4 km away from Genteng. Based on the classification by Handley et al. (2007), Kukusan and Genteng are the intra-caldera volcanoes, which erupted between 21 and 2 ka (Sitorus 1990).

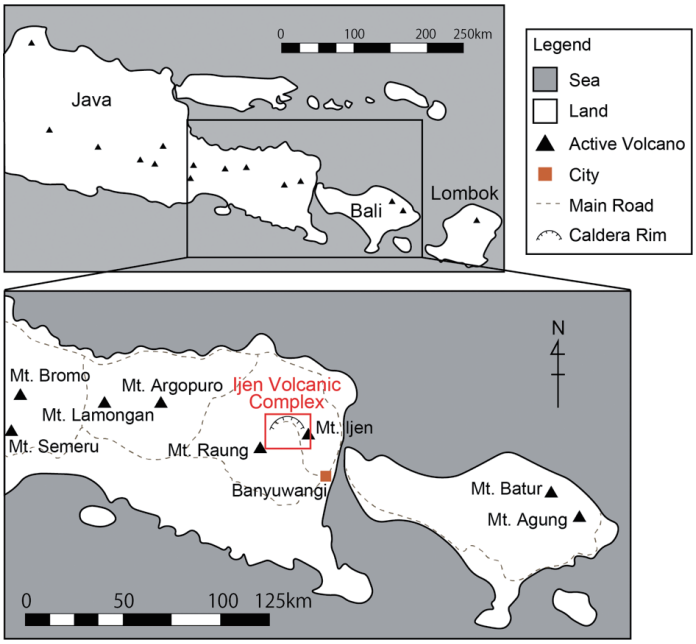

Fig. 1 East Java and Bali regional map. The research area is demarcated by the red box and includes the Ijen Caldera Complex and Mt. Ijen.

III. Methods

Fieldwork was conducted two times in 2018 and once in 2019. Pyroclastic stratigraphy was recognized at 31 locations. The observed units were correlated to draw an isopach map of the pyroclastic deposits. The samples were collected from six locations. The bulk chemical compositions of the major elements were analyzed using a Primus IV X-ray fluorescence spectrometer (Rigaku Corporation). In slightly weathered rock samples, the weathered part was removed before the analysis. Grain size distribution (GSD) was measured in the laboratory of Petrology and Volcanology, Kyushu University with sieves ranging from 32 to 1/2 mm ($ø_{GSD}$ from -5 to 1 on the $ø_{GSD}$ scale of Walker 1971). We manually selected the 8-16 mm juvenile clasts for the component analysis. The color, morphology, vesicularity, and bubble size of juveniles were observed by the naked eye. Several 8-16 mm scoria clasts were randomly selected for bulk density analysis. The scoria volume was measured using a 3-D scanner (Solutionix D700), whereas an electric scale (Shimadzu UW420S) was used to estimate the scoria weight. Bulk density of each scoria was calculated using its weight and volume. A few representative clasts from each volcano were selected: maximum density, minimum density, and modal density. Then, several polished thin sections were produced from the clasts for the petrographic and microtextural analyses.

The microscopic textures were described using electron microscope images. The backscattered electron (BSE) images were acquired at three magnifications: 30×, 100×, and 1000×. The 30× and 100× images were captured using a TM3030Plus scanning electron microscope (SEM) with an accelerating voltage of 15 kV. The 1000× images were taken using a JEOL JXA-8530F field emission electron probe micro analyzer (FE-EPMA) with a prove current of 6 nA and an accelerating voltage of 15 kV. The outlines of the crystals and bubbles were traced manually using Adobe Illustrator (version 24.3). The areas of crystal and bubble were measured using Image J (version 1.52k). Coalesced bubbles were separated into individual bubbles by manual tracing (Fig. 2).

Images at a magnification of 30× were used to observe phenocryst assemblages, vesicularity, and bubble-free phenocryst crystallinity. We took 10-16 images per thin section, and thereby made a large mosaic image using Adobe Illustrator. Crystals with an area over 0.01 mm^2 were considered phenocryst. The fractions of crystal phase, vesicularity, and phenocryst crystallinity in 2-D were calculated using the following equations:

$$fraction\ of\ crystal\ phase_i\ (\%) = \frac{area\ of\ crystal_i}{area\ of\ all\ crystals}\ , \tag{1}$$

$$vesicularity\ (\%) = \frac{bubble\ area}{image\ area}\ , \tag{2}$$

$$crystallinity\ (\%) = \frac{crystal\ area}{image\ area - bubble\ area}\ , \tag{3}$$

where *image area* is the width × length of the BSE image.

Images at a magnification of 100× were used to calculate mean bubble size and bubble number density (BND). Two images of each scoria were taken in different parts of a thin section. The mean bubble size and BND of each scoria were obtained by averaging the measurements from these two images. BND in 2-D ($N_A bub$) was converted to 3-D ($N_V bub$) using the following formula (Toramaru 2019):

$$N_V bub = \frac{N_A bub}{(1 - Ø_{bub}) \times d}\ , \tag{4}$$

where d is the mean equivalent bubble diameter, and $Ø_{bub}$ is the vesicularity in 2-D image. The correction of $1\text{-}Ø_{bub}$ was applied to represent magma conditions before bubble formation in the ascending melt. Although some studies have provided improved formulas to solve the stereological problems (Sahagian and Proussevitch 1998, Higgins 2000, 2002), we favored a much simpler one.

Images at a magnification of 1000× were used to calculate the mean microlite size, microlite number density

(MND), microlite crystallinity, and microlite aspect ratio. Thick sections of each scoria were made for observation with EPMA. Two images of each scoria were taken in different parts. The microlite quantitative data of each scoria were obtained by averaging the measurements from these two images.

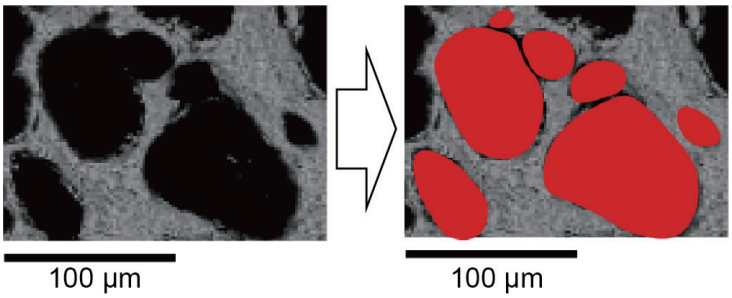

Fig. 2 Part of a 100× BSE image showing an example of coalescence bubbles. Such bubbles were manually traced.

IV. Results

4.1. Stratigraphy of pyroclastic deposits and isopach maps

The pyroclastic deposits of Kukusan volcano were observed at 30 locations (Fig. 3a). Most of these locations are roadcut outcrops represented by scoria, lithic material, and ash. At location I05, the stratigraphic successions (from bottom to top) consist of massive black coarse ash, white fine ash, and two layers of scoria with lithics (Fig. 4a). Both scoria layers are black to brown, loose-packing, and well-sorted. The white fine ash is widely dispersed in the study area. Due to its distinct color (white), we used it as a key layer to correlate stratigraphic columns. The white ash is a product of the Plinian eruption; however, it was derived from an unknown sourced outside of the Ijen volcanic complex (Sundhoro 1990). Similar scoria and white ash layers were observed at locations I13, I17 (Fig. 4b), and I15. The scoria layer thickness increases closer to the Kukusan vent: scoria layer thickness equals 46, 65, 105, and 120 cm at locations I05, I13, I17, and I15, respectively. The scoria layer was also observed inside the Kukusan crater at location I89. The Kukusan scoria dispersed not only to the northern side of the vent, but also to the eastern and north-eastern sides. At locations I73 and I99, the scoria layer is found between two layers of white fine ash (Fig. 4c). The maximum size of the Kukusan scoria was 10 cm at location I13. At some locations, the scoria layer contains cauliflower bombs. The observed scoria clasts are bubble-rich. These bubbles are small (<2 mm), and not elongated. The lithics are red-orange in color. The maximum size of lithics reaches 5.6 cm at location I18. The Kukusan scoria samples were collected at locations I13, I15, I17, I89, and I99. At these locations, the scoria layer was subdivided into two layers (A and C) from bottom to top (Fig. 4a).

The pyroclastic deposits of Genteng volcano were observed only at one location. The outcrop is located on the flank of the Genteng vent at location I43. The stratigraphic successions (140 cm thick) consists of two layers of scoria with rare lithics (Fig. 4d). The scoria layers are black to brown, loose-packing, and well-sorted. The maximum Genteng scoria size is 23 cm. Some scoria clasts are slightly weathered on their surfaces. Most scoria clasts are bubble-rich. These bubbles are relatively larger (up to 1 cm), and not elongated. The scoria layer was subdivided into two layers (A and B) from bottom to top (Fig. 4d). Layer A is a mixture of ash and scoria, while layer B consists scoria only.

The dispersal area of Kukusan scoria is wide compared with that of Genteng (refer to isopach map, Fig. 3a). The Genteng scoria can be found solely on the flank of Genteng volcano. Based on the geomorphology and geological map (Sujanto et al. 1988), we drew a dispersal map for the Genteng scoria (Fig. 3b).

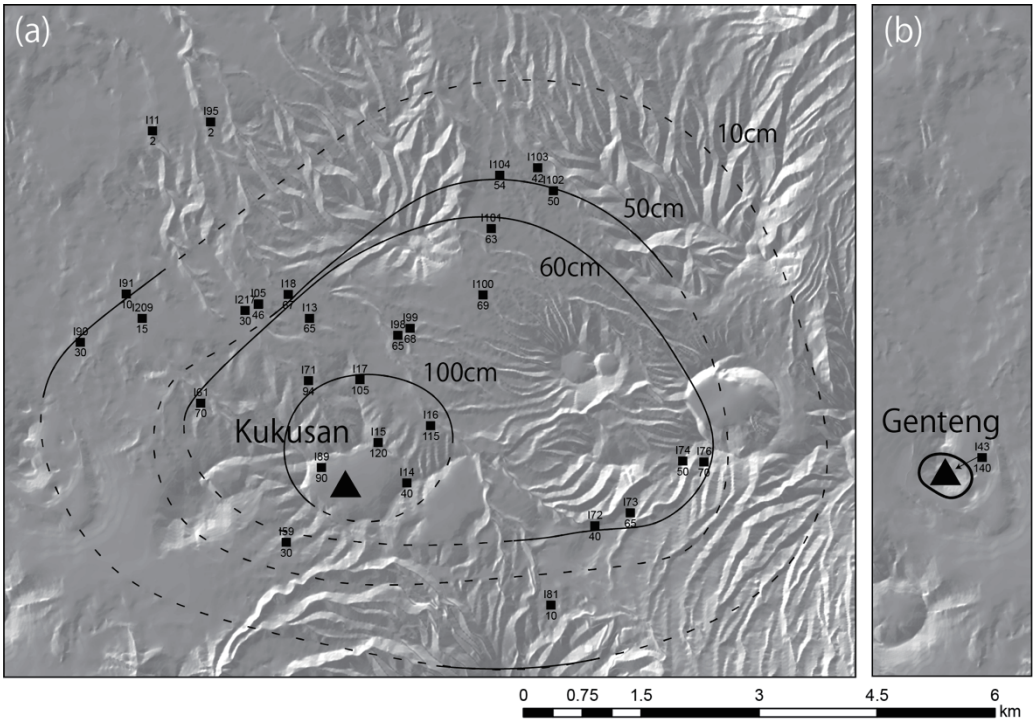

Fig. 3 (a) Outcrop location and dispersal map of the Kukusan scoria. (b) Outcrop location and dispersal map of the Genteng scoria. Black squares—outcrop locations; the number above the black square—location number; the number below the black square—thickness of scoria layer [cm]; black triangles—volcano vent locations; solid line—an isopach; dashed line—an estimated isopach.

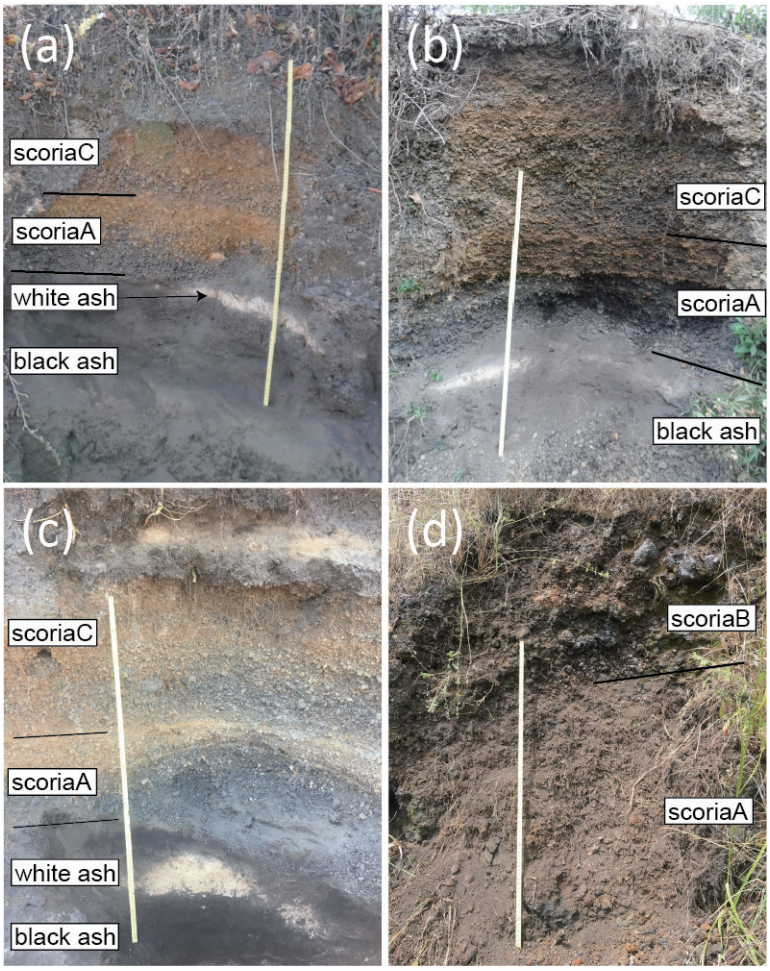

Fig. 4 Photographys of outcrops with volcanic deposits. The length of a measurement stick is 1 m. (a) Kukusan volcanic deposits at location I05. Two scoria layers are underlain by white ash. (b) Kukusan volcanic deposits at location I17. (c) Kukusan volcanic deposits at location I99. (d) Genteng volcanic deposits at location I43.

4.2. Whole rock geochemistry

The SiO_2 content of the Kukusan scoria (52.58 ± 0.5 wt.%) is slightly higher than that published previously (50.23 wt.%) by Sundhoro (1990). Similarly, the SiO_2 content of the Genteng scoria (54.89 ± 0.5 wt.%) is slightly higher than that published previously (53.35 wt.%) by Suhendro et al. (2016). Both the Kukusan and the Genteng scoriae are classified as basaltic andesites (Table 1). Although the chemical composition of the Kukusan magma slightly differs in the SiO_2, Fe_2O_3, and MgO contents from that of Genteng, the overall chemical compositions of the two volcanoes are similar.

Mt.	Location	SiO_2	TiO_2	Al_2O_3	Fe_2O_3	MnO	MgO	CaO	Na_2O	K_2O	P_2O_5	Sum
Kukusan	I89A	52.58	1.02	18.20	10.09	0.18	3.53	7.43	3.23	2.23	0.35	98.84
Genteng	I43B	54.89	1.00	18.23	9.17	0.15	2.58	7.00	3.19	2.31	0.33	98.85

Table 1 Bulk chemical compositions of the Kukusan and Genteng scoriae. Unit: wt.%.

4.3. Grain size

The grain size distribution (GSD) ranges from -6 to 2 on the $ø_{GSD}$ scale in most scoria samples. The Kukusan GSD peaks at -4 to -2 on the $ø_{GSD}$ scale, while Genteng GSD peaks at -6 to -4 on the $ø_{GSD}$ scale (Fig. 5a). The deviation (σ, defined by Walker 1971) among the Kukusan clasts (σ = 0.9-2.0) is lower than that of Genteng clasts (σ = 2.4), meaning that the Kukusan clasts are smaller and better sorted than those of Genteng.

4.4 Component analysis

The Kukusan and Genteng pyroclastic deposits are represented by scoria and lithics. The Kukusan scoria is typically black in color, blocky and ragged in morphology, and is highly vesicular. The bubble size ranges from small (several millimeters) to tiny (cannot be seen with the naked eyes). The Genteng scoria is black to brown in color (appears brown on the surface due to weathering), blocky and ragged in morphology, and is highly vesicular. The bubble size is predominantly small (several millimeters). Thus, the Kukusan and Genteng scoriae can be distinguished from each other based on differences in dominant bubble size. The Kukusan lithic fragments are likely to wall rocks of the volcanic conduit. The Kukusan scoria layer contains 2%-14 % of lithic fragments (Fig. 5b) compared with ~1 % in the Genteng scoria layer.

4.5. Bulk density

The Kukusan scoria at location I89A shows a bimodal density distribution (Fig. 5c). Its maximum density and minimum density are 0.96 and 1.77 g/cm^3, respectively. The Kukusan density distribution peaks at 1.0-1.1 g/cm^3 and 1.4-1.5 g/cm^3. On the contrary, the Genteng scoria at location I43B presents a unimodal density distribution (Fig. 5c). Its maximum density and minimum density are 0.95 and 2.06 g/cm^3, respectively. The Genteng density distribution peaks at 1.2-1.3 g/cm^3.

4.6. Vesicularity and crystallinity

The scoriae of the maximum density, minimum density, and modal density, which was a peak of density distribution, were used for vesicularity and crystallinity observations (termed vesicular, dense, and mode, respectively). Because of the bimodal density distribution of the Kukusan scoria, the scoria corresponding to the smaller density peak was termed modeV, whereas that corresponding to the larger density peak was termed modeD (Fig. 5c).

The Kukusan and Genteng scoria vesicularities range 40-70% and 21-64%, respectively (Table 2). The phenocryst crystallinities of the Kukusan scoria and Genteng scoriae are low and constitute less than 6% and 10%, respectively.

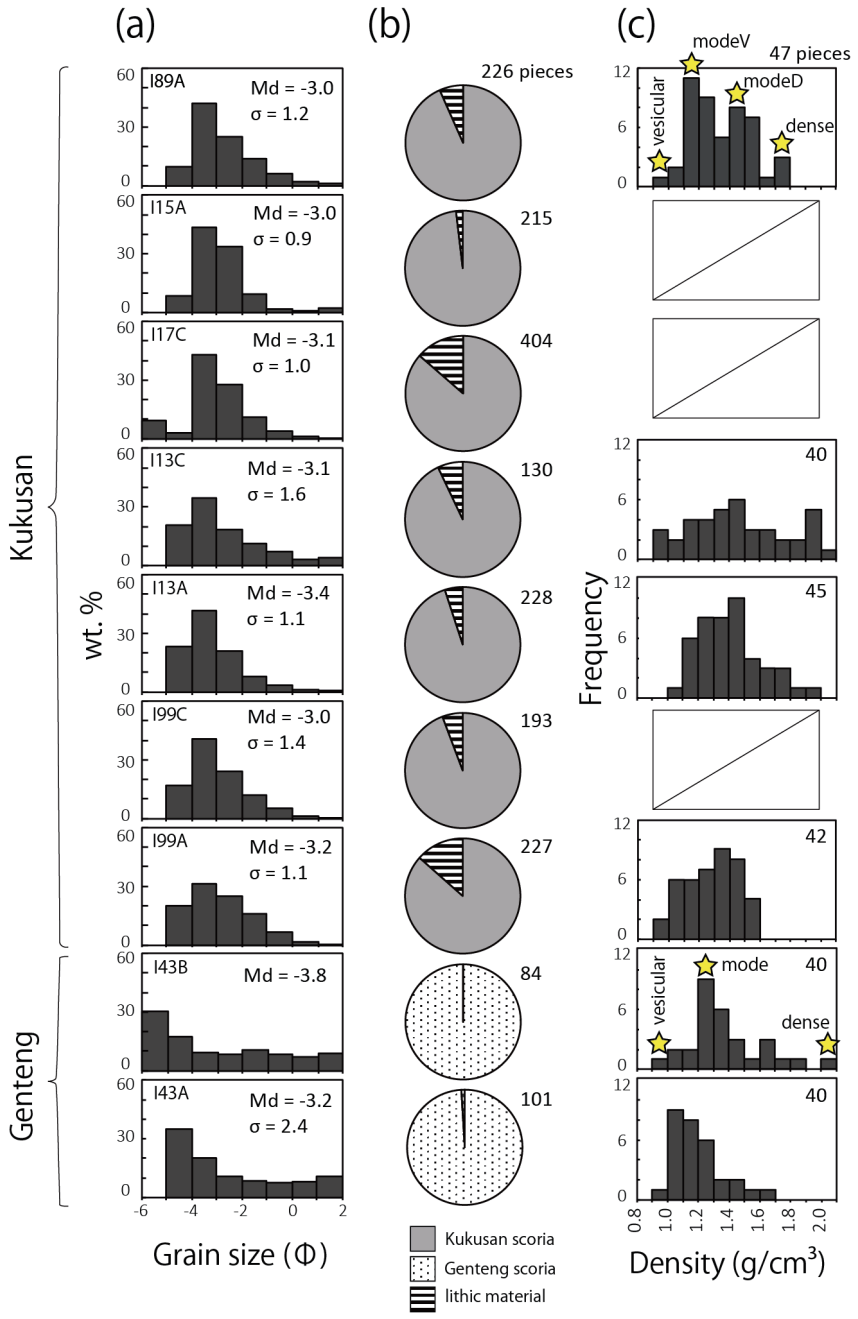

Fig. 5 (a) Grain size distribution of pyroclastic deposits. Md and σ stand for the median diameter and deviation, respectively (Walker 1971). (b) Ratio of scoria and lithic materials in the 8-16 mm clasts. The number above indicates how many samples were analyzed in each sampling location. (c) Bulk density distribution of scoria. The number above indicates how many samples were analyzed in each sampling location.

Mt.	Density category	Density [g/cm^3]	Vesicularity [%]	Phenocryst crystallinity [%]	Fraction of phenocryst phase [%]				
					Pl	Opx	Cpx	Ol	Ox
Kukusan	vesicular	0.96	70	6	72	0	0	25	3
	modeV	1.15	53	4	45	0	0	46	9
	modeD	1.43	41	4	67	0	0	28	5
	dense	1.77	40	6	79	0	0	17	4
Genteng	vesicular	0.95	64	5	95	1	2	0	2
	mode	1.22	49	4	83	11	0	4	2
	dense	2.06	21	10	93	2	5	0	0

Table 2 Density, vesicularity, and phenocryst assemblages of the Kukusan and Genteng scoriae. Density classification: vesicular (minimum density), modeV (smaller density peak of the density distribution), modeD (larger density peak of the density distribution), and dense (maximum density).

4.7. Phenocryst assemblage

Phenocrysts in the Kukusan scoria are composed of plagioclase (Pl), olivine (Ol), and iron-titanium oxide (Ox) (Fig. 6a, Fig. 6b). Pl is subhedral and commonly shows albite twin. Ol is euhedral or anhedral, whereas Ox is euhedral or subhedral. Phenocrysts in the Genteng scoria are composed of Pl, clinopyroxene (Cpx), orthopyroxene (Opx), Ol, and Ox (Fig. 6c, Fig. 6d). Pl is subhedral or euhedral and commonly shows albite twin. Cpx, Opx, and Ol are euhedral or anhedral, whereas Ox is euhedral or subhedral. The Pl fraction in the total phenocrysts in the Kukusan scoria (45%-79%) is lower than that in the Genteng scoria (83%-95%) (Table 2). On the contrary, the Ol fraction in the total phenocrysts in the Kukusan scoria (17%-46%) is higher than that in the Genteng scoria (0%-4%).

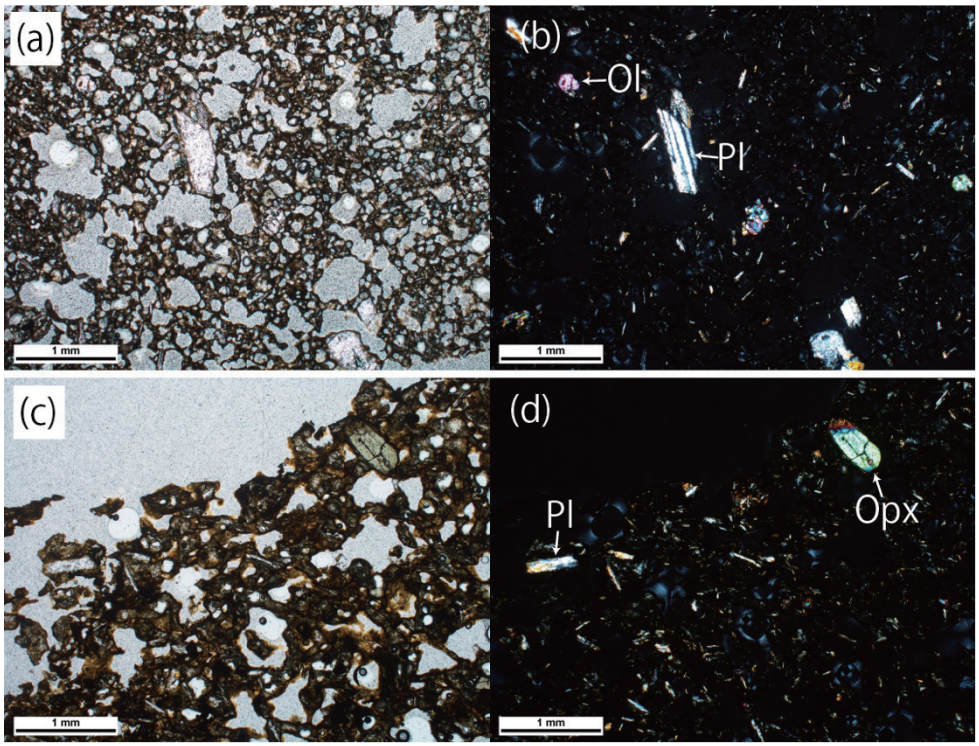

Fig. 6 Petrographic images of scoria. The black bar is 1 mm. Note the phenocrysts of plagioclase (Pl), olivine (Ol), orthopyroxene (Opx), and Fe-Ti oxide. (a) Petrographic image of the Kukusan scoria under open nicol (location I89A). Multiple bubbles are visible. (b) Petrographic image of the Kukusan scoria under crossed nicol. Phenocrysts and micro-phenocryst of Pl are visible. (c) Petrographic image of the Genteng scoria under open nicol (location I43B). (d) Petrographic image of the Genteng scoria under crossed nicol.

4.8. Bubble texture

Based on the qualitative observation of bubbles, the Kukusan and Genteng scoriae are characterized by a microvesicular texture. Most bubble shapes are rounded and connected, indicating bubble coalescence by some extent. The bubbles are not elongated in any direction. The Kukusan scoria contains smaller bubbles and higher BND than the Genteng scoria (Fig. 7). The mean bubble size of the Kukusan scoria (0.034-0.041 mm) is slightly smaller than that of the Genteng scoria (0.049-0.061 mm). The BND of the Kukusan scoria (1.1×10^{13}-3.4×10^{13} m^{-3}) is one order of magnitude higher than that of the Genteng scoria (3.2×10^{12}-4.5×10^{12} m^{-3}) (Table 3).

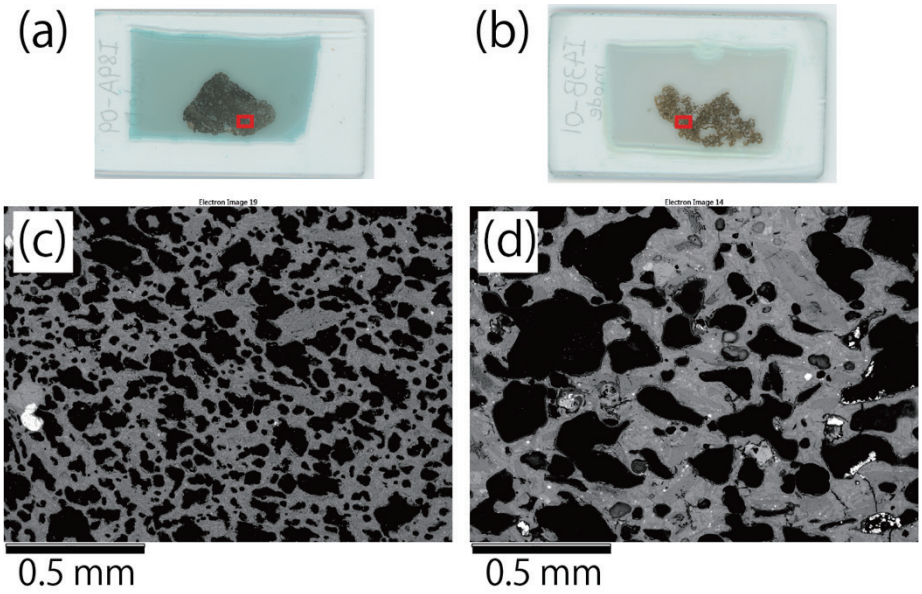

Fig. 7 (a) Scanned thin section of the Kukusan modeD scoria. The red square indicates the approximate location of (c). (b) Scanned thin section of the Genteng mode scoria. The red square indicates the approximate location of (d). (c) 100× BSE image of bubbles in the Kukusan scoria. Black—bubble, gray—glass. Mean bubble size and BND constitute 0.035 mm and 1.9×10^{13} m^{-3}, respectively. (d) 100× BSE image of bubbles in the Genteng scoria. Mean bubble size and BND constitute 0.052 mm and 4.5×10^{12} m^{-3}, respectively.

Mt.	Density category	Bubble		Microlite			
		Size [mm]	BND [no./m^3]	Size [μm]	MND [no./m^2]	Crystallinity [%]	Aspect ratio
Kukusan	vesicular	0.039	34×10^{12}	-	-	-	-
	modeV	0.034	30×10^{12}	3.7	9.1×10^{10}	36	7.5
	modeD	0.035	19×10^{12}	3.8	7.9×10^{10}	41	4.3
	dense	0.041	11×10^{12}	3.8	9.7×10^{10}	48	4.8
Genteng	vesicular	0.061	4×10^{12}	-	-	-	-
	mode	0.052	5×10^{12}	7.9	1.0×10^{10}	29	3.6
	dense	0.049	3×10^{12}	5.0	3.5×10^{10}	31	10.2

Table 3 Mean bubble size, bubble number density, mean microlite size, microlite number density, microlite crystallinity, and microlite aspect ratio of the Kukusan and Genteng scoriae.

4.9. Microlite texture

All studied samples contain abundant microlites. The microlite shows various shapes (Fig. 8). Microlites in the Kukusan scoria are composed of Pl, Px, and Ox. Pl is a tabular or acicular shape; Px is a skeletal or tabular shape; and Ox is an equant shape. Microlites in the Genteng scoria are similarly composed of Pl, Px, and Ox. Pl and Ox have the same shapes as in the Kukusan scoria. Px is octagon or tabular. The mean microlite size of the Kukusan scoria (3.7-3.8 μm) is smaller than that of the Genteng scoria (5.0-7.9 μm) (Table 3). The MND of the Kukusan scoria (7.9×10^{10} m^{-2}-9.7×10^{10} m^{-2}) is higher than that of the Genteng scoria (1.0×10^{10} m^{-2}-3.5×10^{10} m^{-2}). The microlite crystallinity of the Kukusan scoria (36%-48 %) is slightly higher than that of the Genteng scoria (29%-31 %). The mean aspect ratio of the Kukusan scoria (4.3-4.8) is similar to that of the Genteng scoria (3.6-10.2).

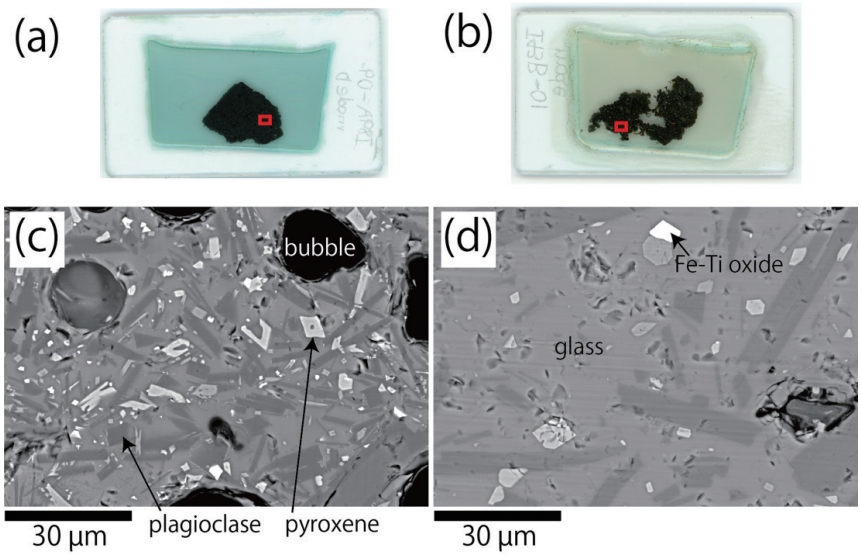

Fig. 8 (a) Scanned thick section of the Kukusan modeD scoria. The red square indicates the approximate location of (c). (b) Scanned thick section of the Genteng mode scoria. The red square indicates the approximate location of (d). (c) 1000× BSE image of microlites in the Kukusan scoria. Mean microlite size, MND, and microlite crystallinity are 3.8 µm, 7.9 × 10^{10} m^{-2}, and 41%, respectively. (d) 1000× BSE image of microlites in the Genteng scoria. Mean microlite size, MND, and microlite crystallinity are 7.9 µm, 1.0 × 10^{10} m^{-2}, and 29%, respectively.

V. Discussion

5.1. Eruption types

The Kukusan and Genteng scoria deposits are loose-packing, well-sorted, and lack accretionary lapilli, suggesting that scoria is a fall deposit and deposited in a dry eruption (Walker and Croasdale 1971). Eruption types are classified by dispersal area (D) and fragmentation degree (F) (Walker 1973). Based on the isopach map constructed herein, the dispersal area of Kukusan is estimated to be 64 km^2 by extrapolating the area enclosed by the 1 cm thickness isopach (Fig. 9), whereas that of Genteng is estimated to be 0.30 km^2 by the dispersal area of Genteng scoria (Fig. 3b). We calculated the fragmentation degree using the weight % of clasts smaller than 1 mm. Based on the grain size analysis results, the fragmentation degree of Kukusan equals 1-7 wt.% at location I13, I15, I89 and I99, whereas that of Genteng equals approximately 16 wt.% at location I43. It should be noted that the fragmentation degree of the Genteng scoria was determined solely from the samples deposited close to the vent. Based on the dispersal area and fragmentation degree, we concluded that the Kukusan eruption type was sub-Plinian, while that of Genteng was Strombolian (Fig. 10).

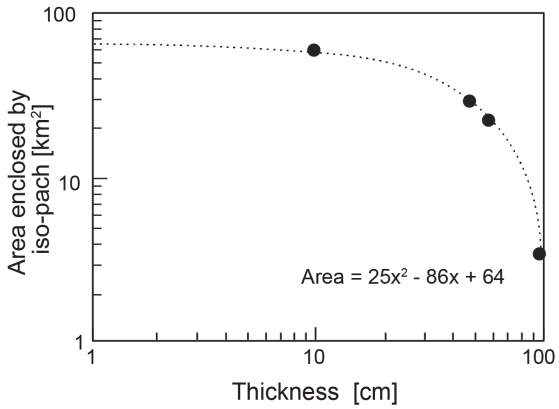

Fig. 9 Area enclosed by the Kukusan isopach against the thickness of the Kukusan scoria deposits. The maximum thickness isopach is 100 cm. The area enclosed by 1 cm isopach is estimated to be 64 km^2 by extrapolation.

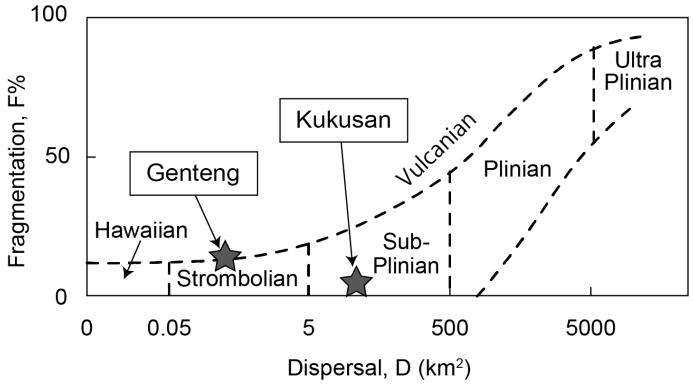

Fig. 10 Diagram showing the classification of eruption types by dispersal and fragmentation (Walker 1973). Kukusan is classified as the sub-Plinian eruption, while Genteng is classified as the Strombolian eruption.

5.2. Comparison with other mafic explosive eruptions

Mafic magma is characterized by various types of explosive eruption type: Hawaiian (Kilauea volcano, USA, 1984-1986), Strombolian (Stromboli volcano, Italy, 2002; Genteng), sub-Plinian (Izu-oshima, Japan, 1986; Kukusan), and Plinian (Etna volcano, Italy, 122 BC). The magmatic compositions of these volcanoes are similar in terms of the SiO_2 content (50-55 wt.%). However, their eruption types differ. It permits us to ask a question, "What is the main factor that influences the eruption type of these volcanoes"?

We compared the BND, MND, and microlite crystallinity of the Strombolian and (sub-)Plinian eruptions using the available data. The BND of Kukusan is similar to that of Etna and Izu-Oshima, and one order of magnitude higher than that of Genteng (Fig. 11). The MND of Kukusan is lower than that of Etna, similar to that of Izu-Oshima and higher than that of Genteng (Fig. 12). The microlite crystallinity of Kukusan is much lower than that of Etna, but similar to that of Izu-Oshima and slightly higher than that of Genteng. Based on these facts, we suggest that BND, MND, and microlite crystallinity correlate positively with the column height and represent the factors that are related to the eruption types (from Strombolian to Plinian).

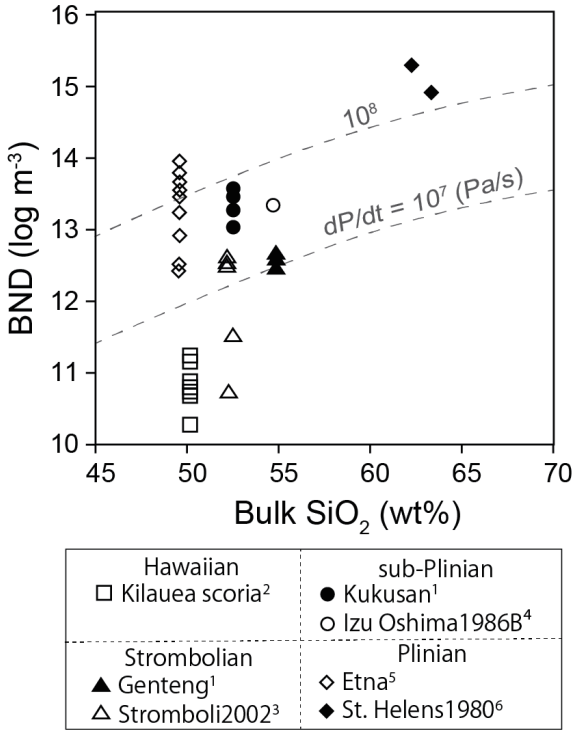

Fig. 11 Comparison of bubble number density for explosive eruption against the magma SiO_2 content. The dashed line is the contour of decompression rate with a water content of 4 wt.%. (Toramaru 2006). References: (1) this study, (2) Mangan and Cashman (1996), (3) Lautze and Houghton (2005, 2007, 2008), (4) Toramaru (2006), (5) Sable et al. (2006), and (6) Criswell (1987), and Klug and Cashman (1994).

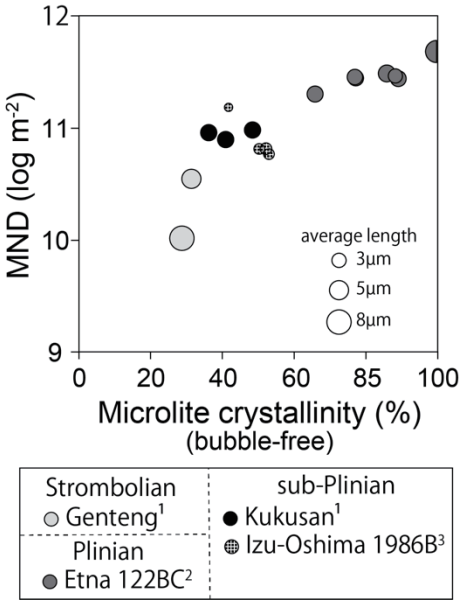

Fig. 12 Comparison of microlite number density for explosive eruption against microlite crystallinity (bubble-free). Symbol size indicates the average length of microlite. References: (1) this study, (2) Sable et al. (2006), and (3) Toramaru et al. (2008).

5.3 Ascent rate

The ascent rate can be regarded as proportional to the decompression rate, assuming steady-state flow conditions. The decompression rate is calculated as a function of SiO_2 and water contents, and BND (Toramaru 2006). The SiO_2 content of Kukusan is similar to that of Genteng with the difference being approximately 3 wt.%. The initial water content of Kukusan and Genteng is unknown: however, it is unlikely to exert a significant influence on the decompression rate (Toramaru 2006). Therefore, we deem that BND influences the decompression rate the most. With the BND of the Kukusan scoria up to one order of magnitude higher than that of Genteng scoria, the Kukusan decompression rate is up to one order of magnitude higher than that of Genteng (Fig. 11).

Microlite crystallization is induced by magma cooling or decompression (Toramaru 2019). Magma temperature is considered almost constant when magma ascends rapidly in the conduit. A rate of water exsolution from a melt, which is proportional to a decompression rate, is calculated as a function of SiO_2 and water contents, and MND, assuming that the water exsolution proceeds at equilibrium (Toramaru et al. 2008). Since pyroxene nucleates homogeneously more than plagioclase (Toramaru 2019), we used pyroxene microlite to calculate MND. The water exsolution rate (dC_w/dt) was calculated using the following formula:

$$\left|\frac{dC_w}{dt}\right| = 2.8 \times 10^{-12-0.23(C_{Si}-50)+0.43C_w} \times (N_V mic)^{\frac{2}{3}}, \tag{5}$$

where $N_V mic$ is the MND of pyroxene; C_{Si} is the SiO_2 content (wt.%); C_w is the initial water content (wt.%). $N_V mic$ was calculated using the following formula:

$$N_V mic = \frac{N_A mic}{d}, \tag{6}$$

where d is the equivalent mean microlite size. $N_V mic$ may have small error because the microlite shape is not typically spherical but rather tabular or square. The pyroxene MND of Kukusan (1.5×10^{13} mm^{-3}) is approximately one order of magnitude higher than that of Genteng (9.9×10^{11} mm^{-3}). The initial water contents of Etna and Stromboli are up to 4 wt.% and 3.4 wt.%, respectively (Houghton and Gonnermann 2008). Since the initial water contents of Kukusan and Genteng were not measured, we assumed a water content of 3 wt. %. The

water exsolution rate of Kukusan (9×10^{-1} wt.% /s) is approximately one order of magnitude higher than that of Genteng (4×10^{-2} wt.% /s). Similar results were obtained for other water contents (1-4 wt.%), suggesting that the decompression rate of Kukusan is much higher than that of Genteng.

The number density of bubbles and microlites demonstrated that the ascent rate of the Kukusan magma is much higher than that of the Genteng magma. There are a few factors to affect an eruption explosivity, i.e. column height (e.g., conduit geometry) (Cassidy et al. 2018). However, a high ascent rate is one of the most important factors that increase the column height. It is suggested that the higher BND and MND values of the Kukusan scoria are related to the cause to induce the highly explosive eruption of Kukusan volcano.

5.4. Viscosity of melt containing microlites

The rheology of magma is essential when considering conduit dynamics. The viscosity of the pure melt phase (η_0) is studied well as Newtonian fluid (e.g., Hui and Zhang 2007) and it can be estimated from temperature (T), water content (C_w) and geochemical composition of the melt. When the magma contains microlites with a range of aspect ratios, it behaves as a non-Newtonian fluid so that the magma viscosity increases. The relative viscosity ($\tilde{\eta}$), which is the microlite-bearing magma viscosity normalized by the viscosity of the pure melt phase, can be estimated from crystallinity ($Ø_{mic}$) and crystal aspect ratio (r_p) (Mader et al. 2013). The aspect ratio significantly affects a maximum packing fraction of crystal ($Ø_{Mmic}$).

In order to assume the temperatures in magma chambers, the chemical compositions of Kukusan and Genteng were applied to Rhyolites-MELTS (v.1.2.0) to calculate liquidus temperature. Assuming a water content of 3 wt.% and constant pressure of 1 kbar (corresponds to a depth of approximately 3 km), the Kukusan magma liquidus equals 1084°C. The magma temperature does not change significantly (1091°C) assuming a water content of 3 wt.% and constant pressure of 2 kbar (corresponds to a depth of approximately 7 km). Under the same conditions of initial water content (3 wt.%) and pressure (1 kbar) as the Kukusan magma, the Genteng magma liquidus equals 1077 °C. In both volcanoes, the magma temperature was assumed to be less than 1100°C. As phenocrysts are thought to be crystallized in the magma chamber, the temperature in the conduit tends to be lower than the liquidus.

We estimated the viscosity of Kukusan and Genteng melt-phase magma (η_0) using the chemical compositions of the Kukusan and Genteng melts for two cases of magma temperatures at 1100°C and 1000°C. The chemical composition of each melt was calculated from the chemical composition of the bulk rock and crystallinity of phenocrysts. For example, the SiO_2 content of each melt was determined using the following formula:

$$SiO_{2\,(melt)} = SiO_{2\,(bulk)} - \sum_i (SiO_{2\,(crystal_i)} \times \text{crystallinity of } crystal_i)\,, \tag{7}$$

where i represents the phenocrysts of Pl, Opx, Cpx, Ol, and Ox. Assuming a water content of 3.0 wt.% and a magma temperature of 1100°C, the melt viscosity of Kukusan was estimated as $\log \eta_0 = 1.9$, while that of Genteng was estimated as $\log \eta_0 = 2.0$. Assuming a water content of 3.0 wt.% and a magma temperature of 1000 °C, the melt viscosity of Kukusan was estimated as $\log \eta_0 = 2.7$, while that of Genteng was estimated as $\log \eta_0 = 2.8$. With similar magma temperatures, the Kukusan and Genteng melt viscosities do not differ significantly. Because the phenocryst crystallinities of Kukusan and Genteng scoriae are low (< 10%), phenocryst may barely affect the melt viscosity.

The relative viscosities ($\tilde{\eta}$) of Kukusan and Genteng microlite-bearing magmas were estimated using the $Ø_{mic}$ and r_p values (Mader et al. 2013). The Kukusan magma behaves as a Herschel-Bulkley fluid because the $Ø_{mic}/Ø_{Mmic}$ ratio exceeds 0.9 (Table 4). Assuming that the strain rate is 1 s^{-1} and the yield stress is 0 Pa, the relative Kukusan viscosity is the second or third power of ten ($\log \tilde{\eta} = 2.1$-3.1). When the yield stress is greater than 0 Pa, the relative viscosity increases. On the contrary, the Genteng magma behaves as a power-law fluid, because the $Ø_{mic}/Ø_{Mmic}$ ratio is 0.6 (Table 4). The relative Genteng viscosity is less than ten ($\log \tilde{\eta} = 0.8$). The effective magma viscosity (η), which is microlite-bearing magma viscosity, is assumed to be a multiplication of the pure melt phase viscosity (η_0) and the relative viscosity ($\tilde{\eta}$). The effective viscosity (η) of Kukusan is 10^4-10^6 Pa s, whereas that of Genteng is 10^3-10^4 Pa s. The microlite crystallinity of the Kukusan scoria (36%-48%) is slightly higher than that of the Genteng scoria (29%-31%). However, the effective viscosities in these two volcanoes differ dramatically. If Kukusan and Genteng volcanoes had the same temperature and initial water content, the effective viscosity of Kukusan should be up to two orders of magnitude higher than that of Genteng.

Volcano	Sample	Crystallinity ($Ø_{mic}$)	Aspect ratio (r_p)	$Ø_{Mmic}$	$\frac{Ø_{mic}}{Ø_{Mmic}}$	log (relative viscosity)
Kukusan	modeV	36%	7.5	0.37	0.97	3.1
	modeD	41%	4.3	0.45	0.92	2.1
Genteng	mode	29%	3.6	0.47	0.61	0.8

Table 4 Relative viscosity of the Kukusan and Genteng microlite-bearing magmas estimated following Mader et al. (2013) and using the microlite crystallinity and aspect ratio.

5.5 Degassing process

We analyze the relationship between degassing in the ascending magma and eruption types by comparing the sub-Plinian eruption in Kukusan and the Strombolian eruption in Genteng. Fig. 13a illustrates a vertical cross-section of a conduit containing a bubble and some microlites during the upward transport of magma. Bubble ascent and expansion tends to be restricted by the high viscosity of the melt. To determine the mobility of bubbles in ascending the melt, it is crucial to examine the bubble ascent velocity relative to the magma ascent velocity. When the bubble velocity is high, decoupled degassing may occur. Conversely, when the bubble velocity is nearly zero, coupled degassing occurs. Assuming a spherical shape of bubbles and a steady-state flow of the melt, the bubble velocity is thought to be the Stokes velocity. The Stokes velocity is negatively proportional to magma viscosity. Because the effective viscosity of the Kukusan magma is higher, the Stokes velocity should be smaller. Therefore, the Stokes velocity in Kukusan is estimated to be low. In addition, since the velocity of magma ascent is quite high, the time available for bubble migration relative to melt is short. Hence, the bubbles may become more immobile in the ascending melt. Consequently, the Kukusan magma undergoes coupled degassing, producing the sub-Plinian eruption (Fig. 13b). Instead, the effective viscosity of the Genteng magma was evaluated to be relatively low. In addition, the mean Genteng bubble size is larger than that of Kukusan. As the Stokes velocity is negatively proportional to magma viscosity and is positively proportional to the square of the bubble size, it is higher in the Genteng magma than in Kukusan one. With the lower ascent rate of the Genteng magma, the bubbles migrate upwards easier in the Genteng magma. Consequently, the Genteng magma undergoes decoupled degassing and loses its explosiveness, producing the Strombolian eruption.

5.6. Fragmentation

The sub-Plinian and Plinian eruptions of mafic magma are thought to be associated with brittle fragmentation (Sable et al. 2006, Houghton and Gonnermann 2008). A crystallization experiment showed that the criteria of fragmentation are given as an initial magma temperature of less than 1100°C, and a crystal content of over 30 %, which corresponds to a magma viscosity of approximately 10^5 Pa s (Arzilli et al. 2019). Applying this criteria to our results, it is found that the Kukusan magma satisfies these conditions: initial magma temperature less than 1100°C; crystal content 36-48%; and magma viscosity 10^4-10^6 Pa s. Even though the initial magma temperature of Genteng is similar to that of Kukusan, the crystallinity of Genteng is lower than that of Kukusan. Thus, the Genteng effective viscosity is low and is probably insufficient to cause fragmentation. Therefore, the Genteng magma could not reach fragmentation, unlike the Kukusan magma.

VI. Conclusions

- Based on the dispersal area and fragmentation degree of scoria, we argue that the eruption types of Kukusan and Genteng volcanoes are sub-Plinian and Strombolian, respectively.
- The microtextural analysis shows that the Kukusan scoria has a higher bubble number density, microlite number density, and microlite crystallinity than the Genteng scoria. Assuming the same water contents, the ascent rate and effective viscosity of the Kukusan magma are higher than those of the Genteng magma.
- We ascertain that the eruption type of basaltic andesite magma is related to its rapid magma ascent and magma viscosity. The higher ascent rate and viscosity of the Kukusan magma cause coupled degassing and fragmentation, leading to a more explosive sub-Plinian eruption. Conversely, the lower ascent rate and viscosity of the Genteng magma cause decoupled degassing, leading to the Strombolian eruption.

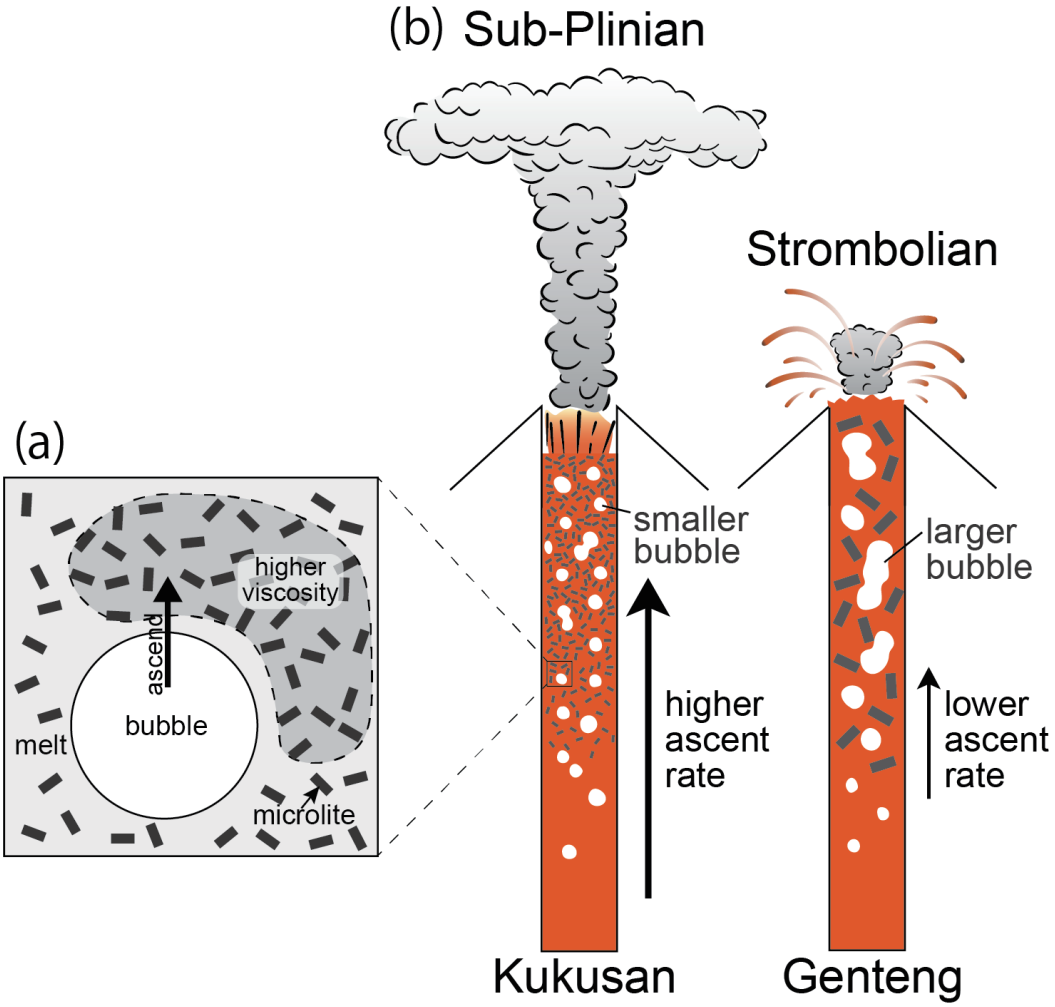

Fig. 13 (a) Vertical cross-section of a conduit (schematic) containing a bubble, some microlites, and melt. High microlite crystallinity increases the melt viscosity and suspends the bubble ascent. (b) Sketch of the Kukusan and Genteng conduits. Higher ascent rate and higher effective viscosity of the Kukusan magma cause bubble immobility relative to the melt. The effective viscosity is high so that reaches magma fragmentation. Lower ascent rate and lower effective viscosity of the Genteng magma make bubbles ascend easier.

Acknowledgements

The authors are grateful to T. Miyamoto, K. Shimada, and Sariyanto for helping with sample analysis. We thank T. Ikeda for his critical comments to clarify this work. We thank M. Nishiwaki and G. N. R. Bunga Naen for their fieldwork help. We also thank M. Ohashi for his helpful review of the manuscript and relevant comments.

References

Arzilli, F., La Spina, G., Burton, M. R., Polacci, M., Le Gall, N., Hartley, M. E., Di Genova, D., Cai, B., Vo, N. T., Bamber, E. C., Nonni, S., Atwood, R., Llewellin, E. W., Brooker, R. A., Mader, H. M. and Lee, P. D. (2019) Magma fragmentation in highly explosive basaltic eruptions induced by rapid crystallization. *Nature Geoscience*, **12**(12), 1023–1028.

Cassidy, M., Manga, M., Cashman, K. and Bachmann, O. (2018) Controls on explosive-effusive volcanic eruption styles. *Nature Communications*, **9**(1), 2839.

Caudron, C., Syahbana, D. K., Lecocq, T., Van Hinsberg, V., McCausland, W., Triantafyllou, A., Camelbeeck, T., Bernard, A. and Surono (2015) Kawah Ijen volcanic activity: a review. *Bulletin of Volcanology*, **77**(3), 16.

Costantini, L., Houghton, B. F. and Bonadonna, C. (2010) Constraints on eruption dynamics of basaltic explosive activity derived from chemical and microtextural study: The example of the Fontana Lapilli Plinian eruption, Nicaragua. *Journal of Volcanology and Geothermal Research*, **189**(3–4), 207–224.

Criswell, C. W. (1987) Chronology and pyroclastic stratigraphy of the May 18, 1980, eruption of Mount St. Helens, Washington. *Journal of Geophysical Research*, **92**(10), 237–266.

Hamilton, W. B. (1979) *Tectonics of the Indonesian region*. Washington, DC, 345pp.

Handley, H. K., Macpherson, C. G., Davidson, J. P., Berlo, K. and Lowry, D. (2007) Constraining fluid and sediment contributions to subduction-related magmatism in Indonesia: Ijen Volcanic Complex. *Journal of Petrology*, **48**(6), 1155–1183.

Higgins, M. D. (2000) Measurement of crystal size distributions. *American Mineralogist*, **85**(9), 1105–1116.

Higgins, M. D. (2002) Closure in crystal size distributions (CSD), verification of CSD calculations, and the significance of CSD fans. *American Mineralogist*, **87**(1), 171–175.

Houghton, B. F., Wilson, C. J. N., Del Carlo, P., Coltelli, M., Sable, J. E. and Carey, R. (2004) The influence of conduit processes on changes in style of basaltic Plinian eruptions: Tarawera 1886 and Etna 122 BC. *Journal of Volcanology and Geothermal Research*, **137**(1-3 SPEC. ISS.), 1–14.

Houghton, B. F. and Gonnermann, H. M. (2008) Basaltic explosive volcanism: Constraints from deposits and models. *Chemie der Erde*, **68**(2), 117–140.

Hui, H. and Zhang, Y. (2007) Toward a general viscosity equation for natural anhydrous and hydrous silicate melts. *Geochimica et Cosmochimica Acta*, **71**(2), 403–416.

Kereszturi, G. and Nemeth, K. (2012) Monogenetic Basaltic Volcanoes: Genetic Classification, Growth, Geomorphology and Degradation. *Updates in Volcanology - New Advances in Understanding Volcanic Systems*, 16–17.

Klug, C. and Cashman, K. V. (1994) Vesiculation of May 18, 1980, Mount St. Helens magma. *Geology*, **22**(5), 468–472.

Lautze, N. C. and Houghton, B. F. (2005) Physical mingling of magma and complex eruption dynamics in the shallow conduit at Stromboli volcano, Italy. *Geology*, **33**(5), 425–428.

Lautze, N. C. and Houghton, B. F. (2007) Linking variable explosion style and magma textures during 2002 at Stromboli volcano, Italy. *Bulletin of Volcanology*, **69**(4), 445–460.

Lautze, N. C. and Houghton, B. F. (2008) Single explosions at Stromboli in 2002: Use of clast microtextures to map physical diversity across a fragmentation zone. *Journal of Volcanology and Geothermal Research*, **170**(3–4), 262–268.

Mader, H. M., Llewellin, E. W. and Mueller, S. P. (2013) The rheology of two-phase magmas: A review and analysis. *Journal of Volcanology and Geothermal Research*, **257**, 135–158.

Mangan, M. T. and Cashman, K. V (1996) Joumalof volcanology and geothermal research The structure of basaltic scoria and reticulite and inferences for vesiculation, foam formation, and fragmentation in lava fountains. *Journal of Volcanology and Geothermal Research*, **73**(1–2), 1–18.

Sable, J. E., Houghton, B. F., Del Carlo, P. and Coltelli, M. (2006) Changing conditions of magma ascent and fragmentation during the Etna 122 BC basaltic Plinian eruption: Evidence from clast microtextures. *Journal of Volcanology and Geothermal Research*, **158**(3–4), 333–354.

Sahagian, D. L. and Proussevitch, A. A. (1998) 3D particle size distributions from 2D observations: Stereology for natural applications. *Journal of Volcanology and Geothermal Research*, **84**(3–4), 173–196.

Sitorus, K. (1990) Volcanic stratigraphy and geochemistry of the Idjen Caldera Complex, East Java, Indonesia. *Unpublished MSc thesis, University of Wellington, New Zealand*.

Suhendro, I., Harijoko, A. and Bunga Naen, G. N. R. (2016) Karakteristik Batuan Hasil Gunung Api Dalam Kaldera (Intra Caldera) Ijen, Desa Kalianyar, Kecamatan Sempol, Kabupaten Bondowoso. *Unpublished Boucher thesis, Gadjah Mada Universitiy, Indonesia*.

Sujanto, Syarifuddin, M. Z. and Sitorus, K. (1988) *Geological Map of the Ijen Caldera Complex, East Java*. unpublished.

Sundhoro, H. (1990) A study of the stratigraphy, volcanology and geochemistry of proclastic rocks from the Ijen caldera complex, East Java, Indonesia. *Unpublished MSc thesis, University of Wellington, New Zealand*.

Toramaru, A. (2006) BND (bubble number density) decompression rate meter for explosive volcanic eruptions. *Journal of Volcanology and Geothermal Research*, **154**(3–4), 303–316.

Toramaru, A., Noguchi, S., Oyoshihara, S. and Tsune, A. (2008) MND(microlite number density) water exsolution rate meter. *Journal of Volcanology and Geothermal Research*, **175**(1–2), 156–167.

Toramaru, A. (2019) *Vesicularion and Crystallization of Magma: Fundamentals of the Volcanic Eruption Process*.

Tokyo University, 493pp.
Walker, G. P. L. (1971) Grain-Size Characteristics of Pyroclastic Deposits. *The Journal of Geology*, **79**(6), 696–714.
Walker, G. P. L. (1973) Explosive volcanic eruptions - a new classification sheme. *Geologische Rundschau*, **62**(2), 431–446.
Walker, G. P. L. and Croasdale, R. (1971) Characteristics of some basaltic pyroclastics. *Bulletin Volcanologique*, **35**(2), 303–317.